

CFD Modelling of Alumina Feeding

Kristian Etienne Einarsrud, Sindre Engzelius Gylver and Eirik Manger

Abstract The dissolution and distribution of alumina in molten cryolite bath is a complex process, involving heat and mass transfer, phase transition and dynamics for a particle population with variable size and properties. Although single particle models can describe essential features of the process, they necessarily fail to capture features involving the interaction between particles (i.e. collisions and adhesion) and detailed coupling to the flow field, for which computational fluid dynamics (CFD) is needed. Several strategies and assumptions have been proposed in the literature, focusing on separate phenomena of relevance. Coupled models considering the full history of alumina particles have however not yet been developed. In the current work we investigate and review recent developments in coupled CFD particulate flow, aiming for general guidelines for implementation and use, with applications to both the gas-solid flow between the feeder and bath surface, and from the bath surface to dissolved alumina.

Key words: Alumina feeding · Agglomeration · Dissolution · CFD Modelling

1 Introduction

The dissolution and distribution of alumina in a molten cryolite bath is a complex and coupled process, involving simultaneous heat and mass transfer, phase transi-

Kristian Etienne Einarsrud

Norwegian University of Science and Technology (NTNU), Department of Materials Science and Engineering, Trondheim, Norway, e-mail: kristian.e.einarsrud@ntnu.no

Sindre Engzelius Gylver

Norwegian University of Science and Technology (NTNU), Department of Materials Science and Engineering, Trondheim, Norway, e-mail: sindregy@stud.ntnu.no

Eirik Manger

Hydro Aluminium, Primary Metal Technology, Norway e-mail: Eirik.Manger@hydro.com

tion and agglomerate dynamics. As pointed out by Dassylva-Raymond et al. [1], the formation of agglomerates affects the overall dissolution (and distribution) of alumina as well as cell stability. Evidently, a deeper understanding of these phenomena is of interest for further development of Hall-Héroult process.

As pointed out in the recent review by Lavoie et al. [2], successful operations rely upon additional features in addition to dissolution, namely delivery (i.e. feeding), dispersion and distribution.

Starting from the delivery of alumina to the cell, the size of the alumina particles must be of such a nature that the particles are able to reach the bath, as pointed out by Lavoie et al. [2]. Small particles will more easily be affected by the hot gas that rises from the feeder hole and this part of the dose will ultimately spread as dust.

Considering well dispersed alumina grains reaching the bath surface, a frozen bath layer will form on the (cold) particle - resulting in a heat transfer dominated regime prior to the mass transfer dominated dissolution [3]. The highly dynamic aggregate will evolve and move depending upon local thermo- and hydrodynamic conditions - ideally becoming fully dissolved and distributed before the next dose is added.

For larger particle doses, the alumina will spread on the bath surface, resulting in an aggregate consisting of particles and frozen bath. These so called rafts have a complex structure consisting of solidified bath, alumina infiltrated with bath and dry alumina [4]. During the heating of the raft, the alumina can undergo a phase transition, resulting in sintering of alumina grains [5]. The fate of the raft is governed by the local thermo- and hydrodynamic conditions, ultimately resulting in smaller agglomerates or lumps. As pointed out by Thonstad et al. [3], apart from the sintering and lump formation, it is possible to use general theory to elucidate probable mechanisms and dissolution rates. This has been demonstrated by Dassylva-Raymond [1], essentially by adopting a single particle model to describe the evolution of a single agglomerate.

Further refinements have been developed by Kaszas et al. [6], treating the conditions for which alumina particles float or sink into the bath, indicating that the angle of repose, bulk density and specific surface area (BET) are crucial.

Although the single grain and agglomerate models describe the essential features of the dissolution process, features involving the interaction between particles forming the agglomerates (i.e. collisions and adhesion) and coupling to the flow field is not covered by such approaches. As pointed out in the pioneering work of Kaszas et al. [4] - raft formation and its effects have not been thoroughly investigated yet, for instance related to the partitioning between particles which disperse and particles which agglomerate. Advanced models based on computational fluid dynamics (CFD) can potentially accelerate the understanding of these phenomena, as demonstrated for anodic gas evolution [7, 8] and for alumina precipitation in the Bayer process [9, 10] over the last decade.

In the current work we review recent developments in coupled CFD particulate flow, aiming for general guidelines for implementation and use, with applications to both the gas-solid flow between the feeder and bath surface, and from the bath surface to dissolved alumina. A detailed review of all features related to particulate flow

is well beyond the scope of the current work - interested readers are recommended to study the recent review of Zhong et al. [11].

2 Model formulations

As indicated in the introduction, modeling the feeding and dissolution process as a whole pose specific requirements to a modeling framework. The framework must allow for three phase calculations, considering particles, gas and molten bath as well as the interaction and interfaces between these. Moreover, the framework must allow for heat and mass transfer, particularly freezing and melting.

There are two main strategies available for the modeling of coupled particulate flows, depending upon the frame of reference used to describe the particulate phase, i.a. Eulerian or Lagrangian. Fluid phases are (almost) always considered in a Eulerian reference frame and particulate flows are thus denoted Euler-Euler or Euler-Lagrange. In both cases, the motion of each phase is described by separate equations, with special coupling term between phases.

In order to simplify the formalism, the presence of more than one phase is modeled with the concept of phase fractions (Drew and Passmann [12]). Definitions vary in the literature, but one intuitive definition is

$$\alpha_k \equiv \frac{V_k}{V} \quad (1)$$

which states that the phase fraction of the k -th phase is the volume occupied by this phase, V_k , divided by the total volume, V , i.e. a phasic volumetric concentration. The volume fraction is subject to the constraint

$$\sum_k \alpha_k = 1. \quad (2)$$

2.1 Euler-Euler formulation

Interpreting the phase fraction as a weighting function between phases, it is possible to formulate a set of transport equations for the system, analogous to the transport equations for a single phase fluid [12]. Mass conservation for the k -th phase can be expressed as

$$\frac{\partial(\alpha_k \rho_k)}{\partial t} + \nabla \cdot (\alpha_k \rho_k \mathbf{v}_k) = \dot{R}_k. \quad (3)$$

where \mathbf{v}_k represents the velocity and \dot{R}_k is the rate of production of component k per unit volume, due to phase changes or chemical reactions, e.g. freezing/melting or dissolution. For a system consisting of N phases, $N - 1$ equations on the form

of equation 3 are solved, the final phase fraction being governed by the constraint given in equation 2.

The Navier-Stokes equations of the k -th phase can be expressed as

$$\frac{\partial(\alpha_k \rho_k \mathbf{v}_k)}{\partial t} + \nabla \cdot (\alpha_k \rho_k \mathbf{v}_k \mathbf{v}_k) = \dot{R}_k \mathbf{v}_{ki} + \nabla \cdot (\alpha_k \mathbf{T}_k) + \alpha_k \rho_k \mathbf{f}_k + \mathbf{M}_{ki}, \quad (4)$$

where \mathbf{M}_{ki} is the force per volume acting on the k -th phase due to interactions with other phases (i.e. drag forces), $\dot{R}_k \mathbf{v}_{ki}$ is a momentum source due to mass sources and \mathbf{f}_k represents the body force density, i.e. gravity. The velocity \mathbf{v}_{ki} represents the velocity at the interface at which mass transfer occurs. Finally, \mathbf{T}_k represents the stress tensor acting on the phase in question, i.e. pressure and viscous stresses. One momentum equation on the form of equation 4 must be solved for each of the phases, yielding a total of $4N - 1$ equations for the system as a whole.

The governing equation for the (specific) internal energy u_k is given as

$$\alpha_k \rho_k \left(\frac{\partial u_k}{\partial t} + \mathbf{v}_k \cdot \nabla u_k \right) = \Phi_k - \nabla \cdot \alpha_k \dot{\mathbf{q}}_k + E_k + \dot{R}_k \tilde{u}_{ki} + \alpha_k \rho_k \phi_k, \quad (5)$$

where Φ_k is the dissipation function, $\dot{\mathbf{q}}_k$ is the (interfacial) energy flux, E_k is an energy exchange term (corresponding to \mathbf{M}_{ki} in equation 4), $\dot{R}_k \tilde{u}_k$ represents energy sources due to mass transfer and ϕ_k is an energy source due to the body forces \mathbf{f}_k .

Finally, considering reactions, the conservation equation for the mass fraction m_k^i of the i -th specie of phase k is

$$\frac{\partial}{\partial t} (\alpha_k \rho_k m_k^i) + \nabla \cdot (\alpha_k \rho_k \mathbf{v}_k m_k^i) = \nabla \cdot (\alpha_k \rho_k D_k^i \nabla m_k^i) + \dot{S}_k^i, \quad (6)$$

where D_k^i is diffusivity of the specie in the mixture of the respective phase and \dot{S}_k^i is the volumetric source of the specie, related to the rate of production of phase k through

$$\dot{R}_k = \sum_i \dot{S}_k^i, \quad (7)$$

where the sum is taken over all species i in phase k .

Considering fluid-fluid systems, the principal challenge lies in modeling the exchange terms between the various phases, for instance drag forces present in \mathbf{M}_{ki} . For particle-fluid flow, there are additional challenges related to modeling the stress tensor \mathbf{T}_{ki} . For the fluid-phase, its understanding is conventional; the stress can be decomposed in pressure and viscous shear stresses. For the solid phase, however, particle-particle interactions must be taken into account, leading to particle pressures and viscosities described by the kinetic theory of granular flow (KTGF) [11, 13].

The particle phase properties are implicit in the Euler-Euler approach in the sense that parameters such as the particle diameter is included only as a coefficient in e.g. the drag force. The properties are characteristic for the phase in question, meaning

that if different particle properties are of interest, then separate phases (with corresponding equations) must in principle be introduced.

Some flexibility in the evolution of a given Eulerian phase can be obtained by introducing population balance modeling (cf. [12]). A population balance model (PBM) is, as the name suggests, a model which deals with the interaction of entities forming a population. For instance, the population can represent dispersed particles flow, in which case the entities represent distinct particle classes, for instance based on volume or diameter. Assuming that N_i particles of class i are present in a volume V , the conservation of the i -th particle number density reads

$$\frac{1}{V} \frac{dN_i}{dt} = \frac{dn_i}{dt} = b_i - d_i, \quad (8)$$

where b_i and d_i respectively represent birth- and death rates for the i -th class. The birth and death of particles are coupled in the sense that an event in one class has consequences for another, for instance, two entities of class i may merge (death) and form one entity of class $i + 1$ (birth). Populations may evolve according to any phenomena of relevance, provided that suitable sub-models can be established for birth and death rates.

The Euler-Euler framework has been used extensively for modeling the multi-phase flow in the Hall-Héroult process. Particular interest to alumina has been given to mixing and distribution of alumina under the influence of the different forces present, e.g. bubble induced motion and MHD [7, 14, 15, 16]. Typically, alumina is not treated as a separate phase but as a specie present in the bath - i.e. assuming well dispersed and distributed alumina grains, with reaction rates adjusted to comply with observed dissolution times [15]. The concept of treating alumina as a specie is extended by Hofer [17] and later by Bardet et al. [18] by introducing a PBM model for alumina grains - thus enabling size dependent dissolution kinetics.

To the authors best knowledge, the first simulations considering alumina as a separate phase were performed by Zhan et al. [19], considering two separate alumina phases representing two different grain classes (small and large) with different properties, moving and dissolving in a bath phase. The modeling approach has later been extended to consider agglomerates [20], albeit without considering the initial formation of these.

The main advantage of Euler-Euler approach is computational convenience. As mentioned, the Euler-Euler framework assumes that the particle phase can be modeled as a fluid with special features, meaning that already established *fluid* models and routines can be used. Moreover, the entire population of particles is considered as a continuous phase, meaning that the full population is governed by a single set of equations governing conservation of mass, momentum and energy. The continuous nature of the Euler-Euler approach necessarily results in the loss of local information e.g. particle position and numbers, as only volume averaged properties (phase fraction and number densities) are available. Although the discrete nature of the population to some extent can be modeled by means of (semi)-empirical relations, the application of a Euler-Euler approach to fundamental issues in particle

laden flows is limited [11]. The alternative is to treat the discrete nature of particles explicitly, as in the Euler-Lagrange formulation described in the following.

2.2 Euler-Lagrange formulation

In the Euler-Lagrange formulations, fluids are considered a (Eulerian) continuum, while particles (or groups of particles) are treated as discrete elements. Owing to the discrete nature of the particles, the Euler-Lagrange formulation is often referred to as discrete element methods (DEM) or discrete particle models (DPM).

The governing equations for the fluid phase correspond to those presented in 2.1 with extended source terms. Equations corresponding to 3 and 4 are in this formulation given as

$$\frac{\partial(\alpha_k \rho_k)}{\partial t} + \nabla \cdot (\alpha_k \rho_k \mathbf{v}_k) = \dot{R}_k + \dot{S}_{k,m} \quad (9)$$

and

$$\frac{\partial(\alpha_k \rho_k \mathbf{v}_k)}{\partial t} + \nabla \cdot (\alpha_k \rho_k \mathbf{v}_k \mathbf{v}_k) = \dot{R}_k \mathbf{v}_{ki} + \nabla \cdot (\alpha_k \mathbf{T}_k) + \alpha_k \rho_k \mathbf{f}_k + \mathbf{M}_{ki} + \dot{\mathbf{S}}_{k,mom}, \quad (10)$$

where $\dot{S}_{k,m}$ and $\dot{\mathbf{S}}_{k,mom}$ respectively represent (volumetric) sources of mass and momentum in the k -th phase, originating from interactions with discrete elements;

$$\dot{S}_{k,m} = \frac{1}{V} \sum_{p \in V,k} \frac{dm_p}{dt} \quad \text{and} \quad \dot{\mathbf{S}}_{k,mom} = \frac{1}{V} \sum_{p \in V,k} \mathbf{F}_{pk}, \quad (11)$$

where the sum is taken over all particles p with mass m_p present in a volume V shared with phase k and \mathbf{F}_{pk} is the *sum* of forces which involve interaction between fluid and particle phases, e.g. drag forces and momentum exchange due to mass transfer.

Detailed closure relations for specific phenomena and flow conditions can be found in Clift et al. [21] and only a brief introduction is given here. In its simplest form, the change in particle mass can be modeled as

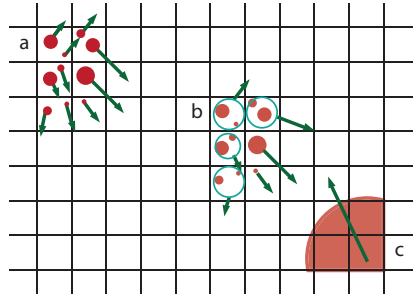
$$\frac{dm_p}{dt} = k' A_p \Delta C, \quad (12)$$

where k' is a mass transfer coefficient, A_p is the particle surface area and ΔC is a concentration difference in bulk and surface concentrations, thus representing a dissolving particle. Corresponding equations can be established for the particle temperature T_p .

The motion of a given particle is governed by Newtons 2. law, i.e.

$$m_p \frac{d\mathbf{v}_p}{dt} = \mathbf{F}_{pk} + \mathbf{F}_p, \quad (13)$$

Fig. 1 Illustration of unresolved (a), particle cloud (b) and resolved particle (c) strategies in the Euler-Lagrange formulation. The computational mesh is indicated with solid black lines.



where \mathbf{v}_p is the particle velocity, \mathbf{F}_{pk} is the total force due to interaction with the fluid phase and \mathbf{F}_p is the total force due to other interactions such as e.g. gravity and particle-particle interactions.

The representation of the forces depends upon the resolution of the numerical method employed (cf. figure 1); unresolved particles are treated as point masses, while the total force on a resolved particle is given by an integral of local contributions. Unresolved particles are thus subject to average flow conditions in a computational region, while resolved particles can be subjected to different conditions depending on e.g. orientation.

To the authors best knowledge, no studies using the Euler-Lagrange formulation for simulation of alumina feeding is available in the open literature, despite the many promising features of the approach.

Since the Euler-Lagrange approach tracks individual particles, such simulations allow for detailed information of the solid face, e.g. particle trajectories, particle-particle-, fluid-particle and particle-free surface interactions [11]. However, the number of equations which needs to be solved is proportional to the number of particles which are to be simulated, making the Euler-Lagrange formulation very resource intensive, easily reaching computational times which are 2 orders of magnitude greater than corresponding Euler-Euler approaches [11]. Particle cloud methods (e.g. particle in cell [22]) aim to reduce this constraint by tracking an ensemble of particles (cf. figure 1b), rather than individual particles, by employing a particle distribution function. According to experiences of Zhong et al. [11], particle in cell methods are typically twice as resource intensive as an Euler-Euler formulation.

2.3 Free surfaces

As demonstrated Kaszas [4, 6], the interaction between alumina particles and the bath surface is of high importance and must be included in a modeling framework aiming to describe the complete feeding and dissolution process.

Various numerical models have been developed to simulate flows separated by immiscible fluid interfaces, the most widely adopted being the Volume of Fluid-(VOF) [23] and the Level Set [24] methods. Both are based on an Eulerian frame-

work with special sub-routines for identification and evolution of the free interface. The various free surface methods have been studied and used extensively due to their many industrial applications such as bubble flow and metal heaving [7], and solidification [25], the latter of which being of particular interest for the current application.

Besides challenges related to computational resources, there are no barriers prohibiting the coupling of the mentioned free surface models to a particle phase like DEM, as demonstrated by Sun and Sakai [26] for an isothermal system without mass transfer. To the authors best knowledge, extensions to systems with (coupled) heat and mass transfer have not yet been reported in the open literature, although the required separate sub models are readily available.

3 Demonstration

In the following section a demonstration of the capabilities of coupled VOF-DPM simulations is given. For simplicity, simulations are performed for isothermal conditions without mass transfer aiming to represent a single non-spherical alumina particle (or dose) falling on the bath surface. Three different cases are considered in which the density ρ and initial height h_0 relative to the free bath surface is varied.

3.1 Simulation conditions

All simulations presented in the following are performed using ANSYS FLUENT version 18.1.0 (ANSYS Inc., Canonsburg) on a cluster running CentOS 7.1. 20 CPUs (E5-2690) running at 2.90 GHz where used for each simulation.

Simulations are performed using the 3D-double precision pressure-based solver, where gradients are computed with a Green-Gauss cell based method and pressure velocity coupling is performed by the SIMPLE algorithm. The free surface is treated by means of the VOF model, discretized using the Geo-reconstruct-scheme without surface tension activated. Density and momentum equations are solved using the second order upwind scheme, while equations for turbulent kinetic energy and dissipation rate are discretized using the first order upwind scheme. Turbulence is modeled by the Realizable k- ε model.

Time advancement is performed using the first-order implicit scheme with a constant time step of 0.0005 s. All other settings are kept at their default values.

The motion of the alumina particle, assumed to be rigid in the current formulation, is treated by means of the 6DOF solver. The moving/deforming mesh utilities within ANSYS are used, with spring/stretch functionality and remeshing when the cells get too distorted, using standard recommended values. A fixed (extended) boundary layer mesh surrounds the dose, ensuring acceptable mesh quality in this region, cf. figure 2d and 4a and b.

Physical properties adopted for the simulations are given in table 1.

Table 1 Values of physical properties used in simulations.

Property	Symbol	Value	Unit
Particle release height	h_0	Varies	m
Particle volume	V_p	$1.285 \cdot 10^{-6}$	m^3
Particle density	ρ	Varies	kg/m^3
Gas density	ρ_g	1.225	kg/m^3
Bath density	ρ_b	compressible	kg/m^3
Gas viscosity	μ_g	$1.7894 \cdot 10^{-5}$	Pa s
Bath viscosity	μ_b	$1.003 \cdot 10^{-3}$	Pa s

Compressible effects are considered for the bath density, modeled as

$$\rho_b = \frac{\rho_{b,ref}}{1 - \frac{\Delta p}{\beta}}, \quad (14)$$

where $\rho_{b,ref} = 2000 \text{ kg/m}^3$ is a reference density, $\Delta p = p - 1\text{atm}$ is the (local) relative pressure (1 atm being the ambient pressure) and $\beta = 2.2 \cdot 10^4 \text{ atm}$ is the bulk modulus of the bath.

3.2 Geometry and mesh

Simulations are performed on a cylindrical 3D geometry with height and radius 10 cm as shown in figure 2. The geometry is enclosed by solid no-slip walls, except for the upper surface, which is a pressure outlet. The computational mesh consists of 891778 polyhedral elements with maximum and minimum cell volumes of $2.1 \cdot 10^{-9} \text{ m}^3$ and $6.65 \cdot 10^{-12} \text{ m}^3$, respectively. As indicated in figure 2, the mesh is the most concentrated and equipped with a boundary layer around the dose, in order to adequately capture the flow in this region.

3.3 Results

Figure 3 shows the evolution of the dose center of mass for three different situations. There are two cases where the dose is released from an initial height h_0 of 2.7 cm. Particle densities are set to 800 and 1200 kg/m^3 , corresponding to doses sizes of 1 and 1.5 g, respectively, and thus reflecting the expected range of densities for a given dose. In the final case a dose of 1 g released is from 5.2 cm above the bath surface. The detailed evolution of the latter case is illustrated in figure 4.

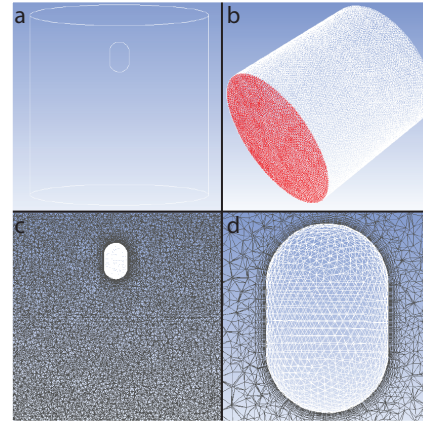


Fig. 2 3D cylindrical geometry used (a) for simulations with details of computational mesh; full volume (b), 2D section (c) and details around and on surface of dose (d).

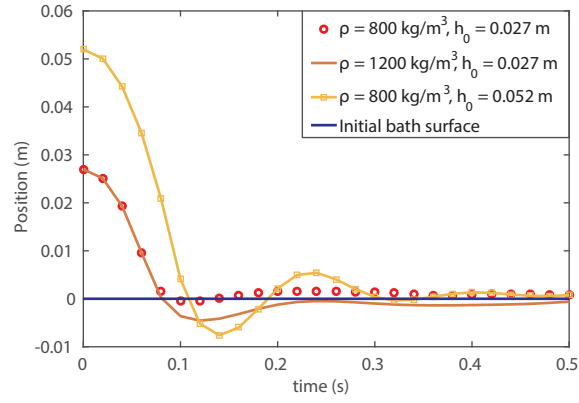


Fig. 3 Position of dose center of mass for three different conditions; low and high density (red circles and brown solid line) and low density released for a greater initial height (yellow squares on solid line). The initial (undisturbed) bath surface is indicated by the solid blue line.

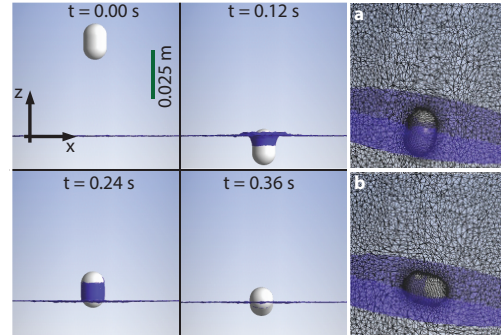


Fig. 4 Motion of dose with density $\rho = 800 \text{ kg/m}^3$ released from $h_0 = 0.052 \text{ m}$. The interaction between the particle and bath interface shows complex behavior due to the multiple degrees of freedom present in the problem. Frames a and b show the mesh corresponding to $t=0.12$ and $t=0.36 \text{ s}$, respectively.

Each of the simulations presented took approximately 2 hours to complete. As seen from figure 3, the two doses with the same mass relax to the same height towards the end of the simulation, whereas the larger mass (higher density) is found at greater immersion - as expected. The particle released from the largest elevation

reaches the bath surface at a greater velocity than the other two cases, penetrating deeper into the bath and will experience different wetting and freezing conditions. As seen in the $t = 0.24\text{s}$, the dose entrains a considerable amount of liquid while emerging from the bath surface. Although the interaction with an actual dose and the interface is different (a real dose will spread and not retain the oblong shape used here), the frames clearly illustrate the complex interactions that might be of importance and thus necessary to include in a modeling framework based on unresolved particles.

4 Discussion and concluding remarks

This paper summarizes various strategies for CFD simulations of alumina feeding and demonstrates the applicability of the VOF-DEM framework for a simplified system.

Considering the specific needs for accurately modeling feeding and formation/evolution of agglomerates, the resolved Lagrangian particle method appears to be a promising approach. Resolved particles can be treated with an arbitrary level of detail, in principle being able to treat phenomena such as freezing and capillary attraction. The drawback of such an approach is that it is CPU intensive, in particular if several particles are introduced. Nevertheless, such an approach, paired with tailored experiments can provide true insight and valuable input to models aiming for computational speed at the cost of details.

Simulations of three different cases using this simulation strategy have been performed and are presented in the current work. The simulations, although very simplified with respect to the phenomena present in an actual feeding situation, demonstrate the potential of the method and reveal complex interactions such as differences in immersion based on both physical and operational conditions and liquid entrainment upon emersion. These properties will most likely have an impact upon freezing and raft formation and thus upon the further dispersion and dissolution process.

For large scale simulations, i.e. those aiming to simulate the actual feeding process involving a multitude of particles, particle cloud methods appears to be a promising approach, being less CPU intensive than other approaches, while retaining some of the essential features relating to the discrete nature of the particles. Identification and quantification of what the essential features are and how they should be implemented is however expected to be challenging. It is however our opinion that considerable insight can be gained by addressing these challenges.

Acknowledgements The current work was funded by the Norwegian Research Council through SFI Metal Production.

References

1. Dassylva-Raymond, V., Kiss, L.I., Poncsak, S., Chartrand, P., Bilodeau, J.-F., Guerard, S.: Modeling the behaviour of alumina agglomerate in the Hall-Héroult process. In: Grandfield, J. (ed.) Light Metals 2014, pp. 603-608. Wiley, Hoboken (2014)
2. Lavoie, P., Taylor, M. P., Metson, J.B.: A Review of Alumina Feeding and Dissolution Factors in Aluminium Reduction Cells. *Met. Mat. Trans. B* **47**, 2690-2696 (2016)
3. Thonstad, J., Solheim, A., Rolseth, S., Skar, O.: The Dissolution of Alumina in Cryolite melts. In: Bearne, G., Dupuis, M., Tarcy, G. (eds.): Essential Readings in Light Metals Volume 2, pp. 105-111, Springer, Cham, (2016)
4. Kaszas, C., Kiss, L., Poncsak, S., Guerard, S., Bilodeau, J.F.: Spreading of Alumina and Raft Formation on the Surface of Cryolitic Bath. In: Ratvik, A.P. (ed.) Light Metals 2017, pp. 473-478, Springer, Cham, (2017)
5. Østbø, N.P.: Evolution of Alpha Phase Alumina in Agglomerates upon Addition to Cryolitic Melts. Ph.D. Thesis 50, Norwegian University of Science and Technology - NTNU, (2002)
6. Kaszas, C., Kiss, L., Guerard, S., Bilodeau, J.F.: Behavior of powders on the surface of a liquid. In: Hyland, M. (ed.) Light Metals 2015, pp. 639-642. Wiley, Hoboken (2015)
7. Einarsrud, K.E., Eick, I., Bai, W., Feng, Y., Hua J., Witt, P.J.: Towards a coupled multi-scale, multi-physics simulation framework for aluminium electrolysis. *Applied Mathematical Modelling* **44**, 3-24 (2017)
8. Poncsak, S., Kiss, L.I., Guerard, S., Bilodeau, J.F.: Study of the Impact of Anode Slots on the Voltage Fluctuations in Aluminium Electrolysis Cells, Using Bubble Layer Simulator, In: Ratvik, A.P. (ed.) Light Metals 2017, pp. 607-614, Springer, Cham, (2017)
9. Kahane, R., Nguyen, T., Schwarz, M.P.: CFD modelling of thickeners at Worsley Alumina Pty Ltd. *Applied Mathematical Modelling* **26**, 281-296 (2002)
10. Woloshyn, J., Oshinowo, L., Rosten, J.: Digester Design Using CFD, in: Donaldson, D., Raahauge B.E.: Essential Readings in Light Metals, Vol. 1 Alumina and Bauxite. Springer, Cham, 350-355 (2016)
11. Zhong, W., Yu, A., Zhou, G., Xie, J., Zhang, H.: CFD simulation of dense particulate reaction system: Approaches, recent advances and applications. *Chem. Eng. Sci.* **140**, 16-43 (2016)
12. Drew, D.A., Passmann, S.L.: Theory of Multicomponent Fluids. *Applied Mathematical Sciences* **135**, Springer, New York, (1999)
13. Gidaspow, D.: Multiphase flow and Fluidization. Academic Press, San Diego (1994)
14. Feng, Y.Q, Cooksey M.A., Schwarz, M.P.,: CFD modelling of alumina mixing in aluminium reduction cells, In: Lindsay, S.J. (ed.) Light Metals 2011, pp. 543-548, Wiley, Hoboken (2011)
15. Witt, P.J., Feng, Y.Q., Snook, G.A., Eick, I., Cooksey, M., A six chemical species CFD model of alumina reduction in a Hall-Heroult cell, in: Olsen, J.E., Johansen, S.T., (Eds.), Progress in Applied CFD, pp- 39-48, Academic Press, Norway, SINTEF, (2015)
16. von Kaenel, R., Antille, J., Romerio, M. V., Besson, O.: Impact of Magnetohydrodynamic and Bubbles Driving Forces on the Alumina Concentration in the Bath of an Hall-Heroult Cell, in: Sadler, B.A. (ed.) Light Metals 2013, pp. 585-590 , Wiley, Hoboken, (2013)
17. Hofer, T.,: Numerical simulation and optimization of the alumina distribution in an aluminium electrolysis pot. These EPFL no 4469, Ecole Polytechnique Federale de Lausanne (2009)
18. Bardet, B., Foetisch, T., Renaudier, S., Rappaz, J., Flueck, M., Picasso, M.: Alumina dissolution modelling in aluminum electrolysis cell considering MHD driven convection and thermal impact. In: Williams, E. (ed) Light Metals 2016, pp. 315-319. Wiley, Hoboken (2016)
19. Zhan, S., Li, M., Zhou, J., Yang, J., Zhou, Y.: CFD simulation of dissolution process of alumina in an aluminum cell with two-particle phase population balance model. *Applied Thermal Engineering* **73**, 805-818 (2014)
20. Zhan, S., Li, M., Zhou, J., Yang, J., Zhou, Y.: Analysis and modeling of alumina dissolution based on heat and mass transfer. *Transactions of Nonferrous Metals Society of China* **25**, 1648-1656 (2015)
21. Clift, R., Grace, J.R., Weber, M.E.: Bubbles, Drops and Particles (Dover Edition). Dover, New York, (2005)

22. Snider, D.M.: An Incompressible Three-Dimensional Multiphase Particle-in-Cell Model for Dense Particle Flows. *Jou. Comp. Phy.* **170**, 523-549 (2001)
23. Hirt, C.W., Nichols, B.D.: Volume of Fluid (VOF) Method for the Dynamics of Free Boundaries. *Jou. Comp. Phy.* **29**, 201-225 (1981)
24. Sussman, M., Smereka, P., Osher, S.: A Level Set Approach for Computing Solutions to Incompressible Two-Phase Flow. *Jou. Comp. Phy.* **114**, 146-159 (1994)
25. Richter, O., Turnow, J., Kornev, N., Hassel, E.: Numerical simulation of casting processes: coupled mould filling and solidification using VOF and enthalpy-porosity method. *Heat Mass Transfer* **53**, 1957-1969 (2017)
26. Sun, X., Sakai, M.: Three-dimensional simulation of gas-solid-liquid flows using the DEM-VOF method. *Chem. Eng. Sci.* **134**, 531-548 (2015)